Preprint Cambridge Centre for Computational Chemical Engineering ISSN 1473 – 4273

Stochastic solution of population balance equations for reactor networks

William J. Menz, Jethro Akroyd, Markus Kraft

released: May 30, 2013

[1] Department of Chemical Engineering
and Biotechnology
University of Cambridge
New Museums Site
Pembroke Street
Cambridge, CB2 3RA
United Kingdom
E-mail: mk306@cam.ac.uk

Preprint No. 127

Keywords: population balance, networks, psr, coagulation, compartmental model, stochastic weighted algorithms

Edited by
Computational Modelling Group
Department of Chemical Engineering and Biotechnology
University of Cambridge
New Museums Site
Pembroke Street
Cambridge CB2 3RA
United Kingdom

Fax: + 44 (0)1223 334796
E-Mail: c4e@cam.ac.uk
World Wide Web: http://como.cheng.cam.ac.uk/

Abstract

This work presents a sequential modular approach to solve a generic network of reactors with a population balance model using a stochastic numerical method. Full-coupling to the gas-phase is achieved through operator-splitting. The convergence of the stochastic particle algorithm in test networks is evaluated as a function of network size, recycle fraction and numerical parameters. These test cases are used to identify methods through which systematic and statistical error may be reduced, including by use of stochastic weighted algorithms. The optimal algorithm was subsequently used to solve a one-dimensional example of silicon nanoparticle synthesis using a multi-variate particle model. This example demonstrated the power of stochastic methods in resolving particle structure by investigating the transient and spatial evolution of primary polydispersity, degree of sintering and TEM-style images.

Contents

1 Introduction

Population balance modelling has traditionally been applied to modelling particle formation in a batch or plug-flow reactor [4, 30, 32]. In the former case, the equations governing particle growth can be simplified to exclude terms for particle transport to- and from the reactor. For the latter case, the reactor model typically represents an axial streamline through the plug flow reactor (PFR). However, there are many systems found in engineering where advective or diffusive particle transport is important [25, 35]. This typically requires use of computational fluid dynamics (CFD) or reactor network approach, coupled with a population balance model to accurately capture particle dynamics.

Solutions for the population balance equation in these coupled systems may be grouped into several classes, the most common of which are monodisperse [11, 22], moment [1, 2, 18, 27] and sectional [40] methods. All of these methods yield a set of differential equations which may solved within the framework of the differential equations describing fluid transport and/or chemical reactions [25].

Many commercial packages now include particle population balances using the aforementioned methods, for example STAR-CCM+ [12], CHEMKIN-PRO [41] and gPROMS [5]. The major drawback of using these methods to solve the population balance equations is that they either do not resolve the particle size distribution (e.g. moments) or utilise a simplified particle model such as a spherical or surface-volume type description. This can cause errors when particle aggregates are formed through coagulation and sintering [29].

There is increasing recent interest in application of stochastic (or Monte Carlo) methods to such systems [25, 35], after the initial work of Garcia et al. [19]. Stochastic methods approximate a real volume of particles by a sample volume of computational particles, where each computational particle represents a certain number of real particles [38, 48]. The idea of a computational particle in the context of a stochastic method is general; and as such, any number of independent particle properties can simulated, for example internal aggregate structure [29, 43, 47] or soot particle composition [15, 33, 44].

Stochastic methods have been applied for simulation of the Boltzmann equations for colliding gas molecules on spatially inhomogeneous domains [9] and adapted to transport of electrons [34]. The key challenge in extending stochastic methods to solve population balances in spatially inhomogeneous systems lies in the simulation of the Smoluchowski coagulation process [35]. In contrast to Boltzmann collisions, Smoluchowski coagulation events reduce the number of computational particles, causing numerical issues.

Implementation of stochastic population balance solvers for flow systems requires discretising the reactor geometry into a mesh composed of reactor 'cells' [25, 35]. These connected cells can be considered a type of reactor network. Kruis et al. [25] developed a 'cell-based weighted random walk' method to account for the movement of particles between cells in a one- and two-dimensional reactor geometry. While reasonably good agreement with a moments code was reported, it was observed that the method was sensitive to stochastic noise, a result of using too few computational particles.

Patterson and Wagner [35] presented a stochastic method for coagulation-advection problems. The performance in accounting for coagulation of the conventional direct simulation algorithm (DSA, [16]) against stochastic weighted algorithms (SWAs, [38]) was

evaluated. It was reported that DSA is particularly susceptible to stochastic noise, which eventually manifests itself as a systematic variance from the true solution.

A study by Zhao and Zheng [52] gave a three-dimensional adaptation of a stochastic population balance solver (using an SWA [53]) coupled with a CFD code. An algorithm was presented to de-couple the fluid flow, particle flow and particle dynamics by choosing an appropriate timestep size. In a similar vein to [25], limits associated with computational cost restricted the maximum number of computational particles, preventing precise agreement with direct numerical simulation (DNS).

'Multizonal' [6, 7] or 'compartmental' models [3, 21, 26, 51] are models in which the fine mesh of CFD is simplified to a coarse network of reactors with a specified flow between each node. Such techniques typically require orders of magnitude fewer reactor cells, thus reducing computational cost, however this comes at the price of decreased spatial resolution of particle dynamics.

Only recently have compartmental models begun to be investigated using stochastic methods: Braumann et al. [10] used a two-reactor dead-zone model and a stochastic algorithm to simulate granulation. Irizarry [21] recently presented an approach to solve a compartmental model with a population balance using a stochastic method. A new algorithm to move particles between cells ('particle bundle flow' method) was reported, in which particles were restricted from jumping more than one compartment by choosing a suitably small timestep. The numerical properties of some test systems were evaluated as a function of the timestep, however the effect of other numerical parameters was not addressed.

There are, however, further open questions in solving reactor networks with stochastic population balance solvers. In order to maximise efficiency of these algorithms, it is necessary to understand the convergence of these algorithms with respect to the number of computational particles and independent runs [46]. Further, it is important to quantify and reduce stochastic noise in the system, as this was identified as a potential issue in [25]. Finally, the coupling of a such a system to a reacting gas-phase has not yet been investigated: this is critical if particle synthesis in real reactors are to be simulated [13, 14].

The purpose of this paper is to extend the work of Irizarry [21], Kruis et al. [25] and Zhao and Zheng [52] by developing an algorithm for solving a fully-coupled gas-phase ODE/particle population balance network. The convergence properties of the stochastic population balance will first be investigated, and methods to reduce statistical error will be considered. The flexibility of stochastic methods in solving the population balance equation will be demonstrated by use of a detailed multivariate particle model to simulate silicon nanoparticle growth in a plug-flow reactor.

The structure of this paper is as follows. In Section 2, the reactor models are presented. The stochastic solution methodology and model used for generating reference solutions are discussed in Sections 2.1 and 2.2 respectively. The numerical test cases and their results are discussed in Section 3. Finally, Section 4 illustrates one of the many ways in which reactor networks can be applied to model a real reactor system.

2 Model description

This work will study the numerical and physical behaviour of a constant-pressure network of perfectly-stirred reactors (PSRs; or continuous-stirred tank reactors, CSTRs). It is assumed that each of these reactors has a characteristic residence time $\tau_{\mathrm{PSR}} = Q/V$ associated with it, where Q is the volumetric flowrate and V is the reactor volume. The creation and interaction of particles with each other in these reactors is described by a population balance equation. The evolution of the number density of particles $n(P)$ of type P is given by

$$\begin{aligned}\frac{\mathrm{d}}{\mathrm{d}t}n(P) = R_{\mathrm{incep}}(\mathbf{c},P) + R_{\mathrm{coag}}(\mathbf{n},P) + \sum_{j=1}^{N_{\mathrm{SG}}} R_{\mathrm{SG},j}(\mathbf{c},P) \\ + \frac{1}{\tau_{\mathrm{PSR}}}\left(\sum_{j=1}^{N_{\mathrm{in}}} f^{[j]} n^{[j]}(P) - n(P)\right) - \psi(\mathbf{c},\mathbf{n},T)n(P)\end{aligned} \tag{1}$$

where $R_{\mathrm{incep}}(\mathbf{c},P)$, $R_{\mathrm{coag}}(n,P)$ and $R_{\mathrm{SG},j}(\mathbf{c},P)$ are the inception, coagulation and surface growth (of growth process j) rates, respectively. The gas-phase expansion factor is given by symbol ψ and the gas-phase species concentrations are given by vector $\mathbf{c}$. The reactor is assumed to have N_{in} inflow streams, each with fraction $f^{[j]}$ of the total volumetric flow. The governing equations for the gas-phase have been discussed in detail elsewhere [13], and are mentioned here briefly for completeness. For N_{GP} gas-phase species, the rate of change in concentration of species k is given by:

$$\frac{\mathrm{d}c_k}{\mathrm{d}t} = \dot{\omega}_k(\mathbf{c},T) + \dot{g}_k(\mathbf{c},\mathbf{n},T) + \frac{1}{\tau_{\mathrm{PSR}}}\left(\sum_{j=1}^{N_{\mathrm{in}}} f^{[j]} c_k^{[j]} - c_k\right) - \psi(\mathbf{c},\mathbf{n},T)c_k \tag{2}$$

where $\dot{\omega}_k(c,T)$ and $\dot{g}_k(c,n,T)$ are the molar production rates of species k at temperature T due to gas-phase and particle reactions, respectively. The gas-phase expansion factor for a PSR is given by

$$\psi(\mathbf{c},\mathbf{n},T) = \frac{1}{\rho}\left(\sum_{k=1}^{N_{\mathrm{GP}}}[\dot{\omega}_k + \dot{g}_k] + \frac{1}{\tau_{\mathrm{PSR}}}\left[\sum_{j=1}^{N_{\mathrm{in}}} f^{[j]}\rho^{[j]} - \rho\right]\right) + \frac{1}{T}\frac{\mathrm{d}T}{\mathrm{d}t} \tag{3}$$

where ρ is the molar density of the mixture. Ignoring energy changes due to the particle population balance, the adiabatic energy balance of a constant-pressure PSR is

$$\rho\overline{C}_{\mathrm{P}}\frac{\mathrm{d}T}{\mathrm{d}t} = \sum_{k=1}^{N_{\mathrm{GP}}}\left(-\hat{H}_k\dot{\omega}_k + \frac{1}{\tau_{\mathrm{PSR}}}\sum_{j=1}^{N_{\mathrm{in}}} f^{[j]}c_k^{[j]}\left[\hat{H}_k^{[j]} - \hat{H}_k\right]\right) \tag{4}$$

where $\overline{C}_{\mathrm{P}}$ is the bulk heat capacity and $\hat{H}_k$ is the specific molar enthalpy of species k.

2.1 Stochastic method

Stochastic methods approximate the real particle system with an ensemble of 'computational particles' [4, 13, 36–38]. The computational particles P_q may interact with each other through a series of stochastic jump processes which define how the particles and the entire population change with time.

2.1.1 Type-space

The type-space refers to the mathematical description of a particle. For the numerical studies in Sections 3 and 4.1, the spherical particle model [29] will be used. In this model, particles of type P are represented as

$$P_q = P_q\left(v^{(q)}\right) \tag{5}$$

where $v^{(q)}$ denotes the volume of the particle q. All other properties (e.g. diameter or surface area) can be straightforwardly calculated from this quantity if the particle density is known. The multivariate 'binary-tree' particle model of Sander et al. [43] is used in Section 4.2, in which the full aggregate structure of a particle is described.

2.1.2 Particle processes

In the stochastic method, the process which create and change particles are typically implemented as jump processes [29]. A brief overview of the adjustments to a particle's type-space due to these processes is given below.

Inception Particles are created in the population balance by inception (also called nucleation). This is represented by the following reaction

$$\mathrm{A} + \mathrm{B} \rightarrow P_q(v_0) \tag{6}$$

where A and B are nucleating gas-phase species. The rate of inception is typically proportional to the gas-phase concentration of these species [28, 30].

Surface growth A surface reaction event may occur in the following manner:

$$P_q\left(v^{(q)}\right) + \mathrm{A} \rightarrow P_q(v^{(q)} + \delta v_\mathrm{A}) + \mathrm{B} \tag{7}$$

where A is a reacting gas-phase species, B is a product species, and δv_A is the volume element added due to the reaction. The rate of reaction is typically described by a Arrhenius expression for a heterogeneous growth process (e.g. [28, 46]), or the free-molecular collision kernel for a condensation process (e.g. [28]).

Coagulation Particles coagulate and stick together according to the following reaction

$$P_q\left(v^{(q)}\right) + P_r\left(v^{(r)}\right) \rightarrow P_s(v^{(q)} + v^{(r)}) \tag{8}$$

The rate of coagulation depends on the choice of coagulation kernel K, which defines the rate at which two particles collide. Both the constant kernel ($K^\mathrm{const} = 1$) and transition kernel (K^tr [23, 31, 37]) are used in the present work.

2.1.3 Algorithms for coagulation

The key challenge in stochastic particle methods is how to solve the Smoluchowski coagulation equation [31]. This work will investigate two popular methods by which this is done: the direct simulation algorithm (DSA, [16]) and a stochastic weighted algorithm (SWA, [31, 38]).

In direct simulation, each computational particle P_q represents the same number of real particles. A coagulation event adds one particle to another, and deletes the unchanged particle from the ensemble. A doubling algorithm [42] is employed in order to prevent depletion of the ensemble, ensuring the actual computational particle count lay in the range $\left[\frac{1}{2}N_{\max}, N_{\max}\right]$.

In stochastic weighted algorithms, computational particles are described by a type P_q and statistical weight w_q. The physical concentration of P_q is then given by w_q/V_{smp}, where V_{smp} is the sample volume, a scaling factor for the ensemble [31]. The coagulation algorithm used in SWAs differs slightly to DSA: after adding the mass of the second particle to the first, the statistical weight of the first particle is changed and the second particle is left unaltered [38]. This is represented by:

$$(P_q, w_q),\ (P_r, w_r) \to (P_q + P_r, \gamma(P_q, w_q, P_r, w_r)),\ (P_r, w_r). \tag{9}$$

where γ is the coagulation weight transfer function, defining how the weight is changed. This work adopts the SWA1 algorithm from [38], where γ is given by:

$$\gamma(P_q, w_q, P_r, w_r) = w_q \frac{w_r}{w_q + w_r} \tag{10}$$

As no particles are deleted in the SWA, there is no need for a doubling algorithm [38].

2.1.4 Flow processes

Previous studies account for particle transport by moving computational particles between cells [21, 52]. Alternative formations for accomplishing this task are presented in the following section. An inflow process uniformly selects a particle of index q from inflow stream j, identifying the particle to be copied into the ensemble. This is represented by the 'reaction'

$$(P_q, w_q)^{[j]} \to (P_r, w_q),\ (P_{r+1}, w_q),\ \ldots,\ (P_{r+F_c}, w_q) \tag{11}$$

where P_r is a copy of P_q, and F_c copies of the particle are made. Note that the particle weights remain unchanged in the inflow process. Adding multiple copies of particles in this manner has the advantage of accelerating the computational particle count $N(t)$ to the maximum value $N_{\max}$, thus preventing depletion of the ensemble (when using the DSA) should the outflow rate be similar. The quantity F_c represents the ratio of the current to inflow ensemble scaling factors:

$$F_c = \frac{V_{\text{smp}}}{V_{\text{smp}}^{[j]}}\ . \tag{12}$$

The rate of an inflow or outflow process is proportional to the number of stochastic particles in the ensemble [8, 13]. For a constant-pressure reactor with constant volumetric

inflow, the rate of inflow from stream j is given as:

$$R_{\text{inflow}}^{[j]} = f^{[j]} \frac{N^{[j]}(t)}{\tau_{\text{PSR}}} \tag{13}$$

where $N^{[j]}(t)$ is the number of stochastic particles in the inflow stream. In this work it is assumed that all reactors have identical values of τ_{PSR}, although the implementation is not restricted to uniform residence times through the network. Two possible implementations of an outflow are now presented. Firstly, upon selection of an outflow jump process, particles can simply be deleted:

$$(P_q, w_q) \rightarrow \text{deleted} \tag{14}$$

The alternative requires consideration of flow processes as 'continuous' rather than as a stochastic jump process. Supposing particles are lost due to an outflow process in time Δt, the ensemble scaling factor V_{smp} can be scaled by factor F_{s} to represent a decrease in the 'real' particle number concentration, as $M_0 = N(t)/V_{\text{smp}}$ [31]. The rescaling factor F_{s} is given by

$$F_{\text{s}} = \frac{1}{1 - \Delta t / \tau_{\text{PSR}}} \tag{15}$$

The new sample volume is simply obtained using $V_{\text{smp}}^{\text{new}} = F_{\text{s}} V_{\text{smp}}$. This form of particle outflow is termed a 'rescale' outflow. It should also be observed that the outflow process of an upstream reactor does not necessarily provide the inflow term of a downstream reactor. The rate of particle outflow from a reactor is given by:

$$R_{\text{outflow}} = \frac{N(t)}{\tau_{\text{PSR}}} \,. \tag{16}$$

The inflow and outflow (in the case of particle deletion) may be included in the stochastic particle method as conventional jump processes (e.g. in Algorithm 2 of [46]). It should also be noted that copying and deletion of computational particles makes tracking of a particle's trajectory through the network challenging.

2.1.5 Coupling to the gas-phase

The stochastic particle method is fully-coupled to a gas-phase ODE solver. The technique of 'operator splitting' is employed to couple the gas- and particle-phases. The algorithm by which this is done (Strang splitting) has been described in detail by Celnik et al. [13] and Shekar et al. [46].

2.2 Discrete Model

In order to assess the numerical properties of the stochastic method, a reliable reference model is needed. In this work, the Discrete Model will be used, which writes the population balance equation as a series of ordinary differential equations (ODEs) [18]. These may be solved using conventional differential equation packages. The Discrete Model is

similar to a sectional method, however every particle size is represented by its own differential equation. Arbitrarily high precision can be obtained by choosing a sufficiently large maximum particle size, corresponding to the number of ODEs N_{ODE}.

For the test particle mechanism, constant inception, surface growth rates will be assumed (with $N_{\mathrm{SG}} = 1$). The rate of coagulation is determined using the Smoluchowski coagulation equation, and is given by [18]:

$$R_{\mathrm{coag}}(n, P_i(v^{(i)})) = \frac{1}{2}\sum_{j=1}^{i-1} K_{j,i-j} n_j n_{i-j} - n_i \sum_{j=1}^{N_{\mathrm{ODE}}} K_{i,j} n_j \tag{17}$$

where $K_{i,j}$ is the coagulation kernel evaluated for particle pair (P_i, P_j). Supposing that particles of size $i \in [1, N_{\mathrm{ODE}}]$ are spherical with volume iv_1, where v_1 is the size of the smallest possible particle, and that coagulation occurs with the constant kernel, the population balance equation is written as

$$\frac{\mathrm{d}n_i}{\mathrm{d}t} = \begin{cases} R_{\mathrm{incep}} - K^{\mathrm{const}} n_i \sum_{j=1}^{N_{\mathrm{ODE}}} n_j - R_{\mathrm{SG}} n_i + \dfrac{1}{\tau_{\mathrm{PSR}}}\left(\sum_{j=1}^{N_{\mathrm{in}}} f^{[j]} n_i^{[j]} - n_i\right) & i = 1 \\ \dfrac{1}{2} K^{\mathrm{const}} \sum_{j=1}^{i-1} n_j n_{i-j} - K^{\mathrm{const}} n_i \sum_{j=1}^{N_{\mathrm{ODE}}} n_j + R_{\mathrm{SG}}\left(n_{i-1} - n_i\right) + \dfrac{1}{\tau_{\mathrm{PSR}}}\left(\sum_{j=1}^{N_{\mathrm{in}}} f^{[j]} n_i^{[j]} - n_i\right) & i > 1 \end{cases}$$

2.3 Solution of reactor networks

The formulation of the above flow processes permits linking of reactors in a generic manner. To solve the transient response of the network, a simple sequential procedure is adopted. This is typically termed 'sequential modular simulation', and similar approaches have been used in other applications [52]. The algorithm employed to solve the fully-coupled gas-phase ODE system with the stochastic population balance solver for N_{reac} reactors is given in Figure 1.

The algorithm in Figure 1 illustrates the solution methodology for Strang splitting, although in theory any form of coupling (e.g. predictor-corrector [14]) could be used. The accuracy of this algorithm is clearly dependent on choice of a sufficiently small splitting timestep Δt_{s}, which has been investigated elsewhere [21, 52].

3 Numerical studies

In stochastic solutions to the population balance, numerical error can manifest itself in two forms: statistical error and systematic error [13]. The numerical error is affected by the maximum number of computational particles (N_{max}), the number of independent runs (L) and the splitting time-step (Δt_{s}) [13, 31, 46]. The error can be assessed by generating L independent estimates of the particle system, and comparing the macroscopic quantities of the system $m(t)$ for a given set of numerical parameters. Those studied in the present work are given in Table 1.

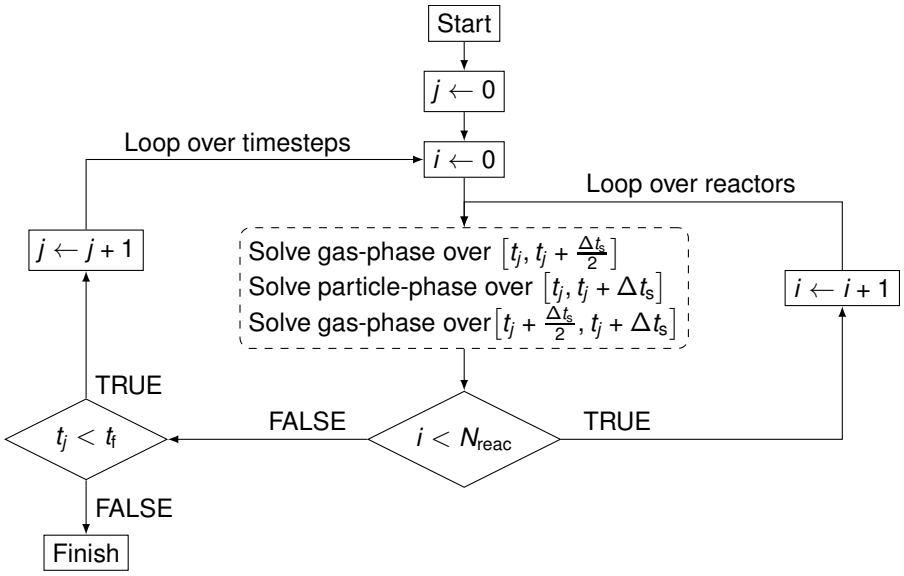

Figure 1: *Algorithm used to solve the reactor network with Strang splitting.*

Table 1: *Summary of process metrics studied in the present work.*

$m(t)$	Description	Formula
$M_0(t)$	Particle number concentration	$\frac{1}{V_{\text{smp}}} \sum_{i=1}^{N(t)} w_i$
$\mu_{\text{a}}(v)(t)$	Average particle volume	$\frac{1}{\sum w_i} \sum_{i=1}^{N(t)} v^{(i)}$
$M_2(t)$	Second mass moment	$\frac{1}{V_{\text{smp}}} \sum_{i=1}^{N(t)} w_i \left(\rho v^{(i)}\right)^2$
$M_3(t)$	Third mass moment	$\frac{1}{V_{\text{smp}}} \sum_{i=1}^{N(t)} w_i \left(\rho v^{(i)}\right)^3$

The temporal evolution of these functionals is averaged over the number of independent runs:

$$\mu^{(N_{\max},L)}(t) = \frac{1}{L}\sum_{l=1}^{L} m_l^{(N_{\max})}(t) \tag{18}$$

The confidence interval c_P for $\mu^{(N_{\max},L)}(t)$ is given by

$$c_{\mathrm{P}}^{(N_{\max},L)}(t) = a_{\mathrm{P}}\sqrt{\frac{\frac{1}{L-1}\left[\sum_{l-1}^{L} m_l^{(N_{\max})}(t)^2\right] - \mu^{(N_{\max},L)}(t)^2}{L}} \tag{19}$$

where P is the confidence level. In this work, $P = 0.999$ is used, for which $a_{0.999} = 3.29$ from normal distribution tables. The total error is then estimated by calculating the relative average absolute error ($\overline{\varepsilon}$) over M time intervals [13]:

$$\overline{\varepsilon}^{(N_{\max},L)} = \frac{1}{M}\sum_{m=1}^{M} \frac{\left|\mu^{(N_{\max},L)}(t_m) - m^*(t_m)\right|}{m^*(t_m)} \tag{20}$$

where $m^*(t)$ is the 'true solution', approximated here as that obtained using the Discrete Model (i.e. the ODE solution). The relative statistical error can be estimated by taking the ratio of the confidence interval and the mean:

$$\varepsilon_{\mathrm{stat}}^{(N_{\max},L)}(t) = \frac{c_{\mathrm{p}}^{(N_{\max},L)}(t)}{\mu^{(N_{\max},L)}(t)} \tag{21}$$

The relative average statistical error may then be obtained:

$$\overline{\varepsilon}_{\mathrm{stat}}^{(N_{\max},L)} = \frac{1}{M}\sum_{m=1}^{M} \varepsilon_{\mathrm{stat}}^{(N_{\max},L)}(t_m) \tag{22}$$

These quantities will be used to analyse the performance of the stochastic population balance solver in simple networks of reactors. As previous work has thoroughly investigated the choice of a correct timestep [21, 52], the focus of the following studies will be on the number of computational particles $N_{\max}$ and the number of independent runs L.

3.1 Comparison to Discrete Model

To test the validity of the stochastic particle algorithm in solving the population balance equations, a simple test system was devised: three reactors connected in series, with possible countercurrent recycle streams opposing the direction of flow. Material is recycled from reactors R2 and R3 with fraction f_{R}, and the total volumetric flowrate Q is constant between all reactors. It was assumed that the inflow to the network contained 1 #/m^3 particles of size $i = 1$, with each reactor having the same residence time τ_{PSR}. A schematic of this system is provided in Figure 2(a).

This system was solved using a simple particle mechanism including terms for coagulation (according to the constant coagulation kernel, $K^{\mathrm{const}} = 1$), surface growth ($R^{\mathrm{SG}} = 1$)

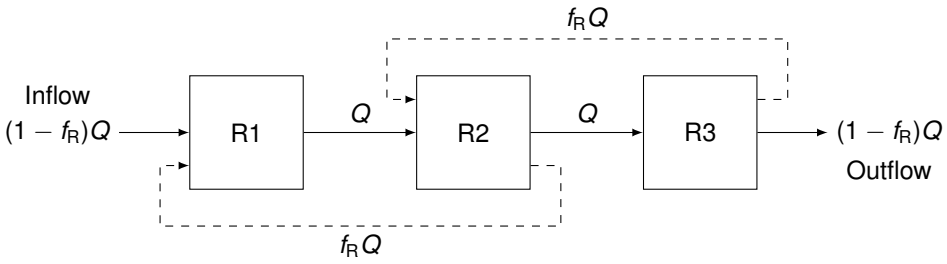

(a) Linear network with recycles

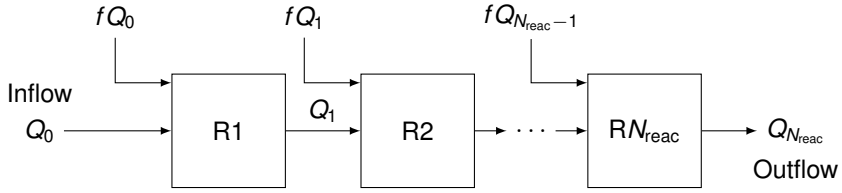

(b) Linear network with multiple inflows

Figure 2: *Schematic of the test systems used in the present study.*

and inception ($R^{\text{incep}} = 1$). While these do not represent physical rate equations, they are helpful for evaluating the performance of the stochastic particle method against other solution methodologies. This was first undertaken by applying the Discrete Model [18] and the stochastic particle method (using the SWA [38]) to solve the test system. The results of this analysis are given in Figure 3, for a linear ($f_R = 0$) and countercurrent (with $f_R = 0.5$) network; and $N_{\max} = 16384$, $L = 8$.

The transient evolution of M_0 illustrates the issue of statistical error present in stochastic solutions to the population balance equation: the 'random' nature of the processes in the stochastic method induce fluctuations in functionals describing the system (e.g. the moments). The noise can be eliminated by averaging the solution over multiple independent runs (i.e. with a different random seed). The influence of this statistical error and systematic variation will be addressed in the following sections.

3.2 Linear networks

As in previous numerical studies into stochastic population balances [13, 31, 46], it is useful to investigate how the error in a stochastic solution varies with the number of computational particles ($N_{\max}$) and independent runs (L). Further, it is likely that the different coagulation algorithms and two outflow process types could contribute different amounts of systematic or statistical error to the stochastic solution.

Using the test case described in the previous section, the stochastic solutions using the DSA and the SWA were generated. It was assumed that reactors R1 and R3 used outflow rescaling as their outflow process, while the outflow process type of R2 was varied. The relative average error in R2 of the stochastic solution with respect to the Discrete Model was evaluated, with a constant $N_{\max} \times L = 10 \times 2^{18}$, and is given in Figure 4.

It is difficult to observe any meaningful differences between coagulation algorithms or

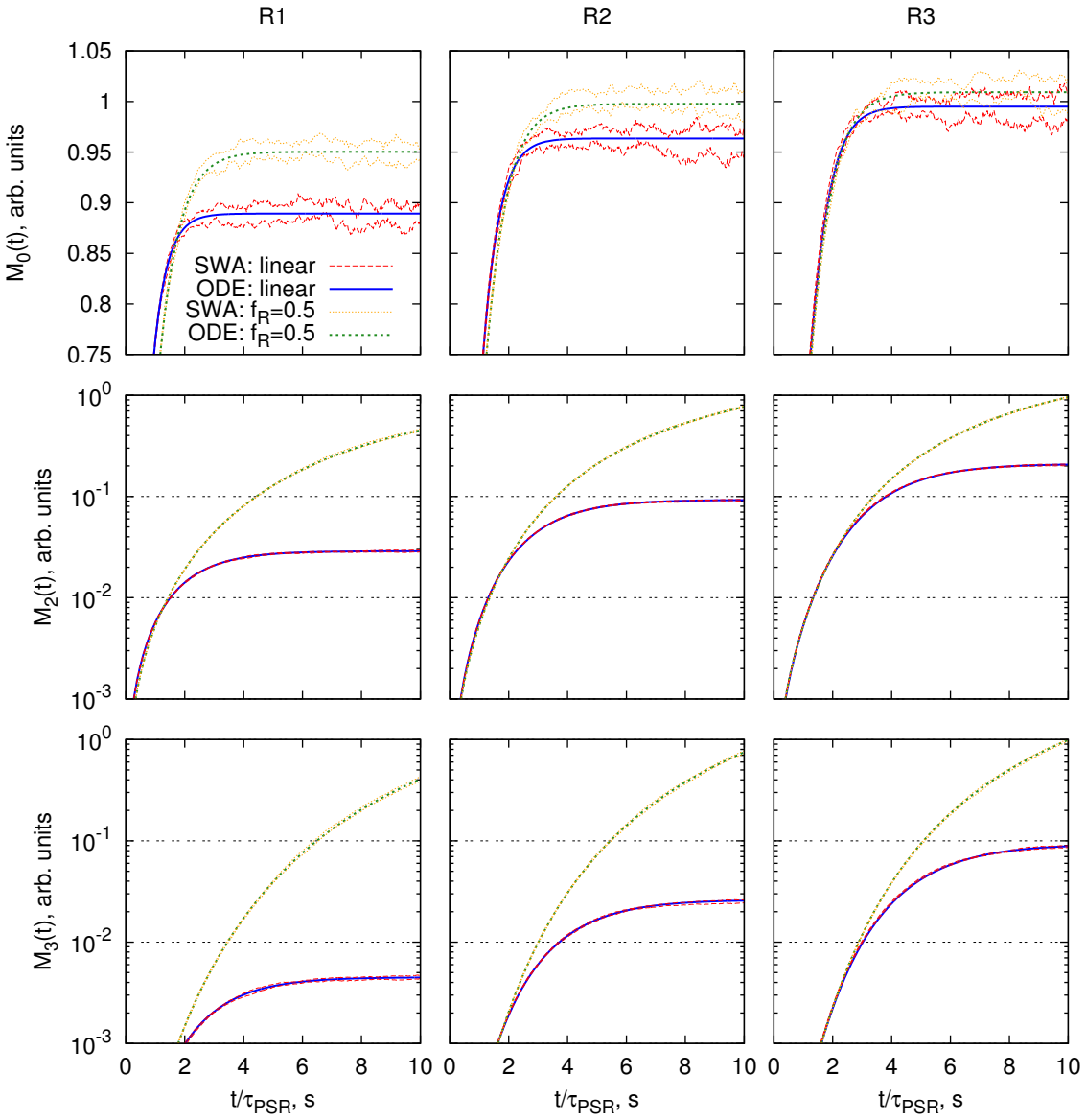

Figure 3: *Comparision of solutions for transient evolution of normalised moments M_0, M_2 and M_3 from the Discrete (ODE) Model [18] and stochastic method (using the SWA) for the three-reactor system (Figure 2(a)) with $f_R = 0$ and $f_R = 0.5$. Confidence intervals of the stochastic solution are given where visible.*

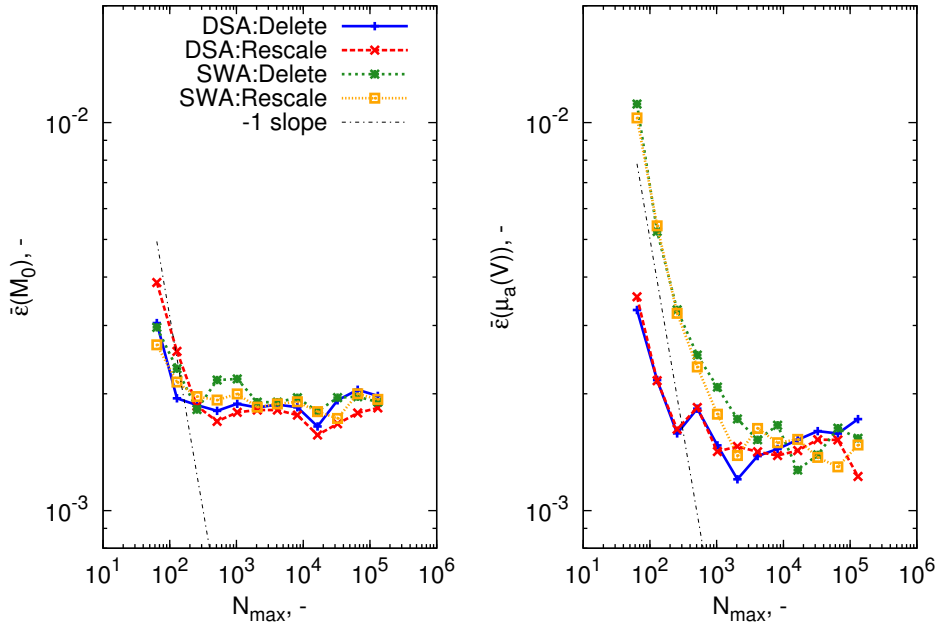

Figure 4: *Convergence of the zeroth moment (M_0) and average volume ($\mu_a(V)$) in R2 using the DSA, SWA; and outflow rescaling and particle deletion.*

outflow processes in examining the error in the zeroth moment (Figure 4, left panel). The approximately flat error indicates that M_0 has converged for all systems by $N_{\max} = 256$, after which the total error is representative of the statistical error. Higher moments (e.g. M_2, M_3) show analogous behaviour. In contrast to this, the error in average particle volume (Figure 4, right panel), and similarly other average particle properties, shows a clear difference between the convergence of the DSA and SWA. Similar behaviour of the SWA was reported in [31].

The previous discussion focused on the reduction of systematic error as a function of numerical parameters. Using Equation (22), the relative amount of statistical error present in each case can also be compared. These results are presented in Figure 5.

Only in the zeroth moment does DSA appear to have a slight advantage in terms of reducing statistical error. For all other cases (particularly the higher moments), the SWA shows up to a 45% reduction in average uncertainty. This is consistent with previous studies [31, 38]. The outflow rescaling process type appears to contribute less statistical error than its particle deletion counterpart. This is unsurprising, since removal of a particle from the ensemble deletes information that could otherwise be preserved in a rescaling approach.

3.3 Networks with recycle loops

Chemical engineering process models may often include a 'recycle stream' [17], where material or energy is transferred from a downstream to an upstream unit operation. The

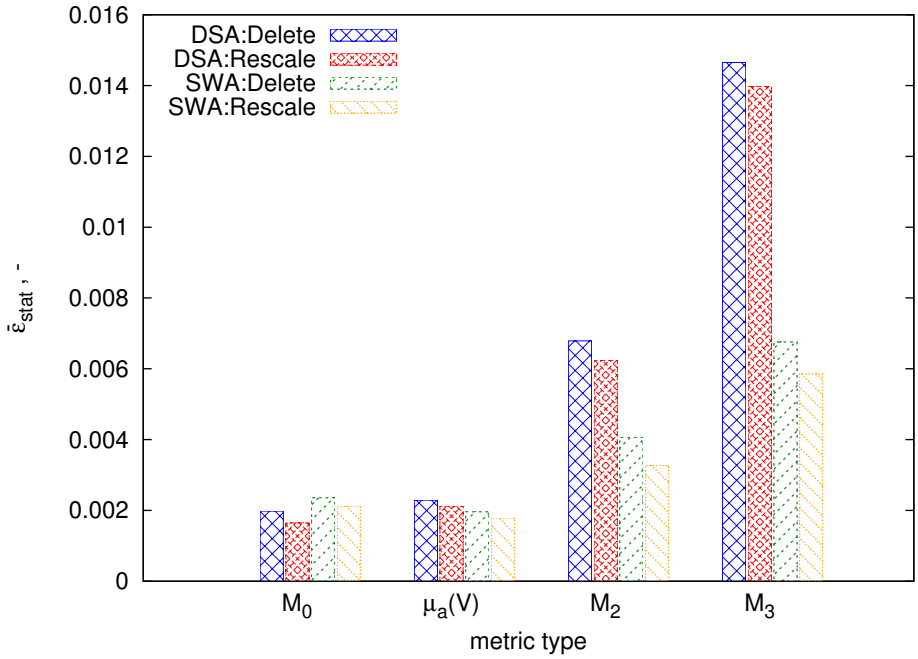

Figure 5: *Comparison of the relative average statistical error ($\bar{\varepsilon}_{stat}$) in key process metrics in R2 ($f_R = 0$) using the DSA, SWA; and outflow rescaling and particle deletion ($N_{max} = 16384$, $L = 160$).*

stochastic solution of the population balance equation has only recently been studied with such networks [21], and as such, this section aims to investigate some of the preliminary characteristics of the stochastic particle algorithm where feedback loops are present.

The relative average error in R2 with respect to the Discrete Model was evaluated for the network in Figure 2(a) using the test particle mechanism with $f_R = 0.5$ ($N_{\max} \times L = 10 \times 2^{18}$); and is presented in Figure 6.

In contrast to Figure 4, it is evident the system is more sensitive to the number of computational particles. The linear decrease in the metrics' average error (slope of -1) with $N_{\max}$ is consistent with other studies of convergence of stochastic particle methods [13, 20, 32]. Only for the zeroth moment does the DSA outperform the SWA for reduction of error as a function of $N_{\max}$. Both methods appear to converge by the same threshold; $N_{\max} = 4096$.

In addition to recycling material (gas-phase and particles), a feedback loop could also recycle statistical error. Using outflow rescaling, the transient evolution of the statistical error in M_3 was evaluated (Equation (21)) in R3 for different values of the recycle fraction. These results are displayed in Figure 7.

As the recycle fraction increases, so does the 'noise' in the solution. Use of the SWA is particularly advantageous in this system, in some cases showing more than an order of magnitude less statistical error than the DSA. The same phenomenon is observed for all other metrics, with the exception of M_0. In the case of M_0, the statistical error is so small that any potential advantage of DSA is outweighed by the error accumulation in the other metrics.

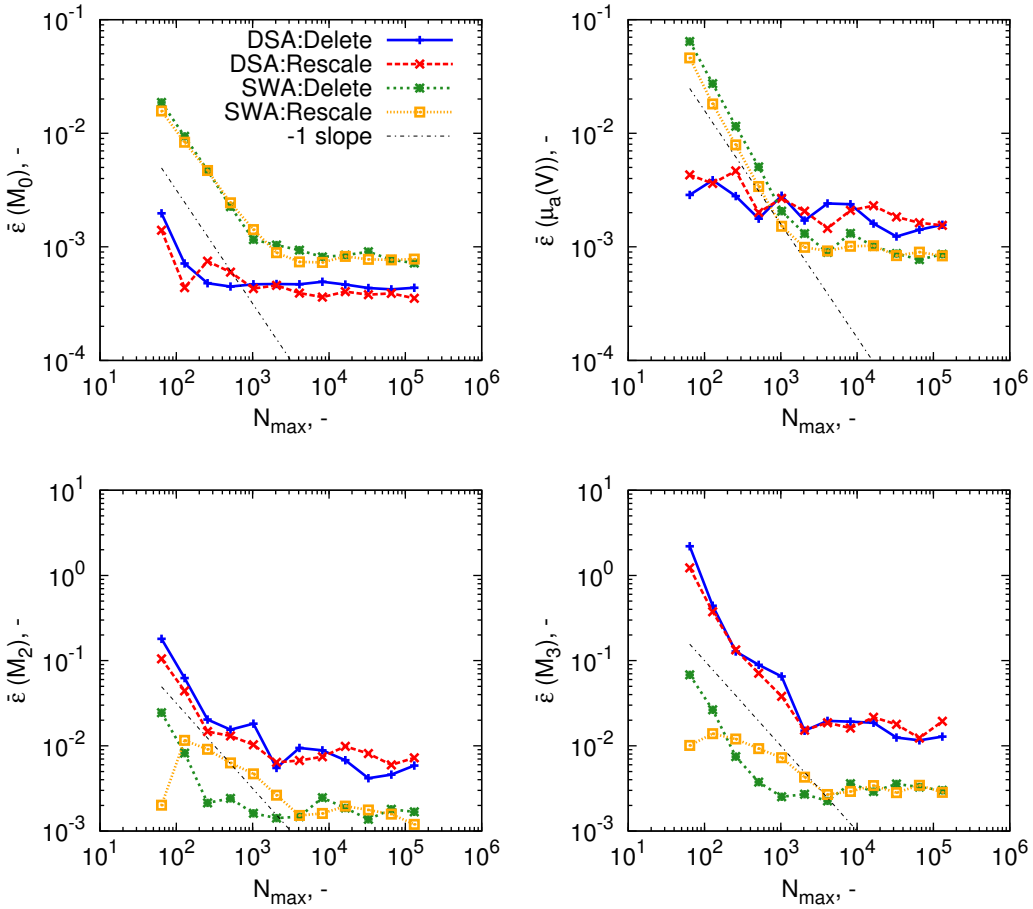

Figure 6: *Convergence of the zeroth moment (M_0), average volume ($\mu_a(V)$) and second and third mass moments (M_2, M_3) for the second reactor (R2) in a countercurrent network with $f_R = 0.5$.*

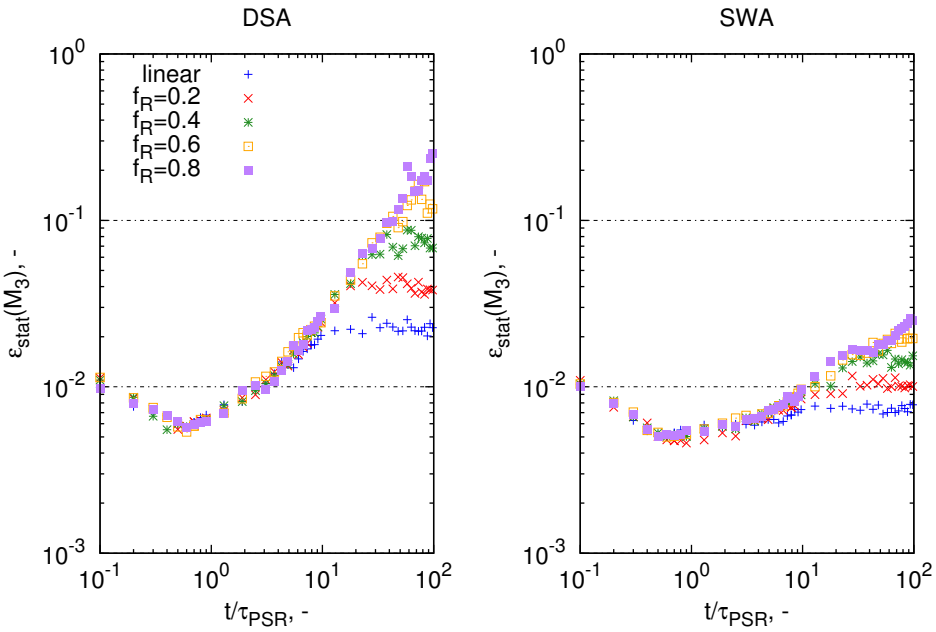

Figure 7: *Normalised statistical error in R3 as a function of dimensionless reactor time and recycle fraction ($N_{max} = 16384$, $L = 160$).*

Although the statistical error appears to stabilise as the reactor reaches steady-state, the statistical error in the DSA solutions is concerningly large; reaching more than 20% for $f_{\mathrm{R}} = 0.8$. In practical use of stochastic population balance modelling, it is uncommon to use 160 independent runs (8 is more common: [28, 46]), as the computational expense can be too great. Since the statistical error is dependent on the number of runs, it is recommended that the SWA be used in place of the DSA for networks with strong feedback.

3.4 Reactors with multiple inlets

The previous analyses addressed linear reactor networks and those which recycle information through the network for a system with three reactors. It is also important to understand the effect of increasing the length of the reactor network and the contribution of material from inflow streams to a reactor. The Damköhler number is typically used to investigate the latter phenomenon, and is defined here as

$$Da = \frac{1/\tau_{\mathrm{coag}}^{\mathrm{in}}}{1/\tau_{\mathrm{PSR}}} \tag{23}$$

where τ_{coag} is the characteristic coagulation time, given by $1/(K^{\mathrm{const}} M_0)$ [29]. By varying the Damköhler number of stream, the effect of an increased coagulation rate upon the test system can be assessed. To do this, the system given in Figure 2(b) with length $N_{\mathrm{reac}} = 10$ reactors and inflow fraction $f = 0.5$ was used. The statistical error in each reactor as a function of inflow Damköhler number was determined and is given in Figure 8.

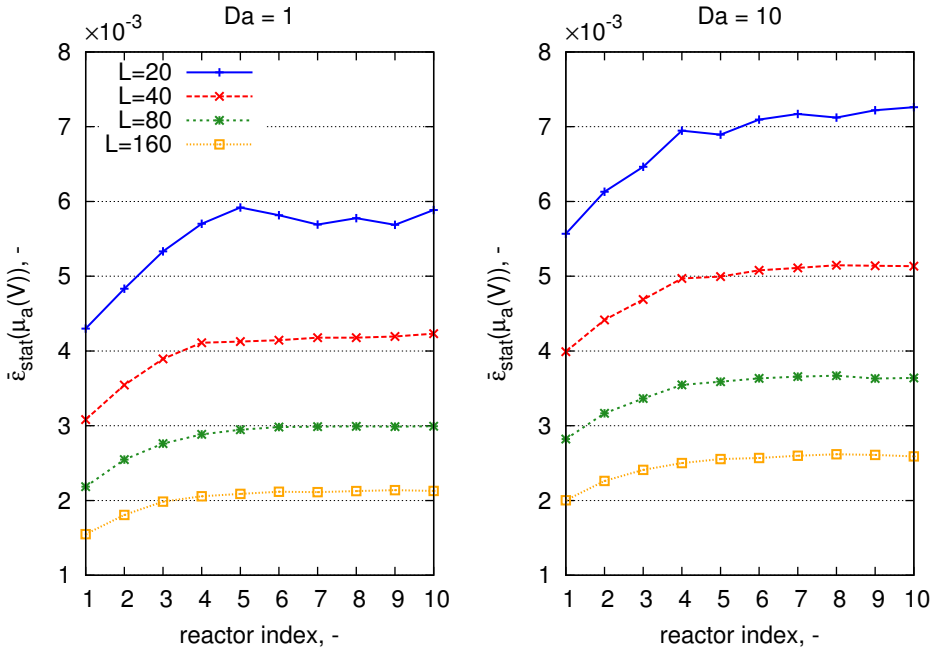

Figure 8: *Normalised average statistical error in the mean particle volume as function of reactor index ($N_{max} = 16384$, SWA coagulation).*

The error measurements increase through the length of the PSR chain, before levelling-off after five reactors. Where more coagulation occurs (higher *Da*, right panel), the error is increased. This analysis illustrates how error can potentially propagate through a reactor chain, although in this particular example the total error is sufficiently low to be of no concern. It is suggested that for systems where particle processes (e.g. coagulation, surface growth) occur over much shorter characteristic times than the transport time, more independent runs or computational particles could be used to offset the accumulation of statistical error.

4 Applications

4.1 Approximation of a PFR

Many aerosol synthesis processes use a tubular hot-wall reactor or similar to manufacture nanoparticles [24, 32, 45, 49, 50]. These processes are typically modelled using a plug-flow reactor (PFR) model, where the length coordinate of the reactor is translated into a time coordinate to permit solution of the population balance equations. However, this formulation does not permit investigation of the transient behaviour of the flow reactor, as the time coordinate is actually in reference to the distance through the reactor.

In development of the plug-flow reactor model, it is typically assumed that the reactor is composed of infinitesimally thin 'plugs'. Supposing that a PFR with constant volume V

has a constant volumetric flowrate Q, the residence time of each reactor is given by:

$$\tau_{\text{PFR}} = \frac{V}{Q} \tag{24}$$

Approximating the PFR as a series of N_{reac} perfectly-stirred reactors, the residence time of each reactor (or plug) is straightforwardly calculated:

$$\tau_{\text{PSR}} = \frac{\tau_{\text{PFR}}}{N_{\text{reac}}} \,. \tag{25}$$

Under this approximation, the ability to model networks of flow reactors with the stochastic particle method therefore permits the transient response of the population balance equations in a PFR to be determined. That is, both the time and the reactor length coordinate can be treated independently. This has practical relevance in reactor start-up and operation.

For practical purposes, it is useful to know how many PSRs are needed to accurately approximate the true PFR solution. This will be a function of the relative timescales of the particle processes with respect to the transport timescale. The Damköhler number is again used to measure the relative influence of coagulation; however here the characteristic transport time τ is taken to be the residence time of the PFR being approximated by the PSR network (i.e. $Da = \tau_{\text{PFR}}/\tau_{\text{coag}}$). To investigate the difference of a network solution to the PFR solution, the 'average PFR error' $\overline{\varepsilon}_{\text{PFR}}$ is first defined. For a reactor network composed of N_{reac} PSRs, each with residence time $\tau_{\text{PSR}}(Da)$; the error in the network's solution with respect to the PFR solution is given by:

$$\overline{\varepsilon}_{\text{PFR}}^{(Da,\ N_{\text{reac}})} = \frac{1}{N_{\text{reac}}} \sum_{i}^{N_{\text{reac}}} \frac{\left| \mu_{\text{R}i}^{(Da)}(t_{\text{SS}}) - m^{*}_{\text{PFR}}(i\tau_{\text{PSR}}) \right|}{m^{*}_{\text{PFR}}(i\tau_{\text{PSR}})} \tag{26}$$

where $\mu_{\text{R}i}$ is the mean of metric $m(t)$ in reactor i of the network over L runs (Equation (18)), and m^{*}_{PFR} the PFR solution for that metric. The number or reactors required to approximate a PFR was studied for a system of particles undergoing a physical coagulation process (transition kernel [31]) with no inception or surface growth. The results for a variety of Damköhler numbers are given in Figure 9. The time required for the network to reach steady-state was empirically found to be $t_{\text{SS}} < 2\tau_{\text{PFR}}$ for all Damköhler numbers.

It is clear that when the relative influence of coagulation is small (low Da), the PSR network approximation to a PFR is valid for very few reactors, and the magnitude of the error is very small. This approximation appears to become less useful as the coagulation process occurs faster, relative to the transport time. It is again illustrated in Figure 10, where the zeroth moment is plotted for various (Da, N_{reac}) pairs.

4.2 Silicon nanoparticle synthesis

To illustrate the application above, the example of Wu et al. [50] is used, where silicon nanoparticles were produced from silane (in N_2) at atmospheric pressure. A multivariate fully-coupled model was recently presented for this system [28], including terms for particle inception, surface growth, condensation, coagulation and sintering.

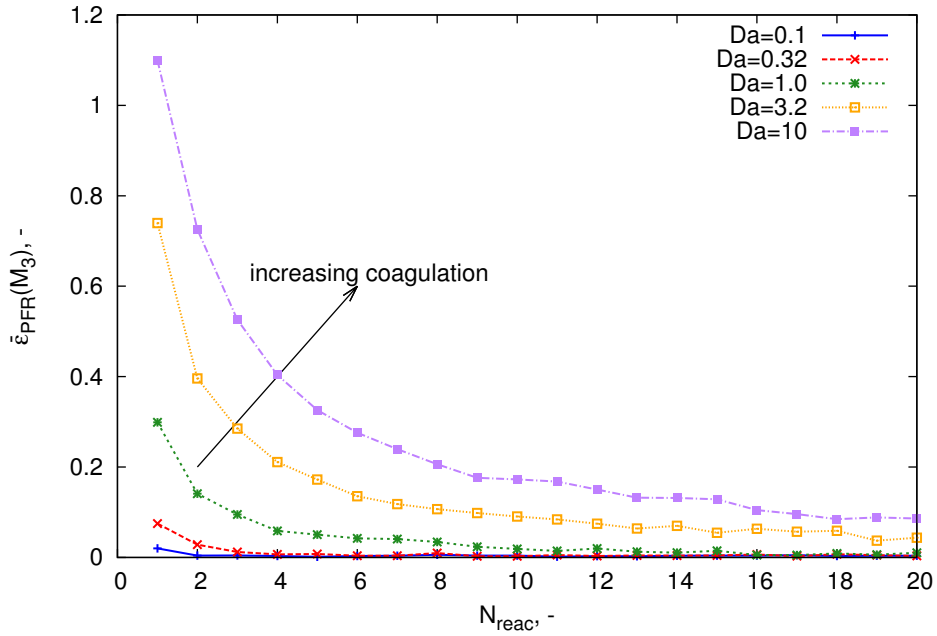

Figure 9: *Normalised average error in M_3 of the networked-PSR solution with respect to the PFR solution for particles undergoing coagulation (transition kernel).*

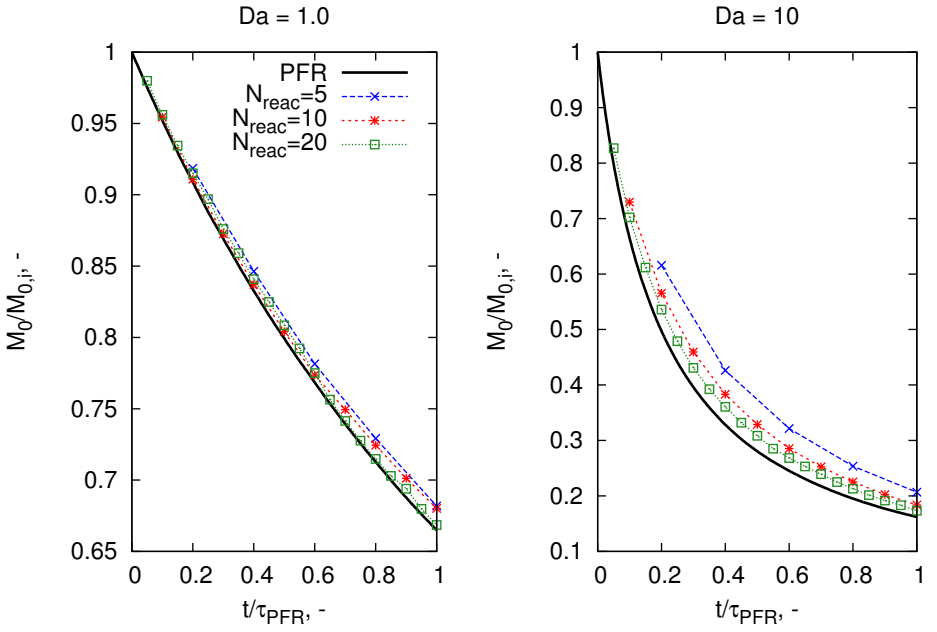

Figure 10: *Temporal evolution of M_0 normalised by its initial value ($M_{0,i}$) of a reactor chain compared to the PFR solution.*

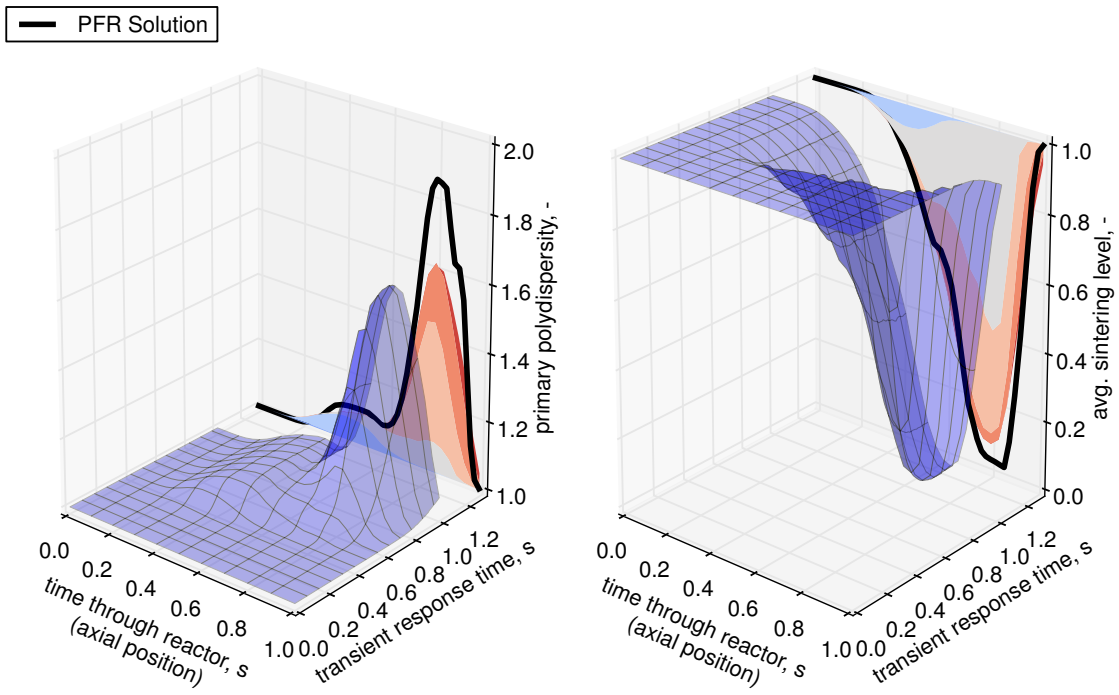

Figure 11: *Mesh plots depicting the transient evolution of the primary polydispersity (given here by the average geometric standard deviation of primary diameter [29]) and the degree of sintering. Contour projections of the network solution are compared to the PFR solution (thick line).*

The fully-coupled gas-particle model was applied to a network of 30 consecutive PSRs, approximating the tubular reactor in [50]. As the reactor configuration used in that study has a length-variable temperature profile, it was assumed that each PSR is isothermal and is of the temperature corresponding to its location along the PFR (i.e. $T_i = T(i\tau_{\mathrm{PSR}})$). Assuming that each PSR was initially filled with inert N_2, the transient response of the PSR network was evaluated, allowing sufficient time for the system to reach steady state. The results of this analysis are given in Figure 11, where the transient and axial evolution of the particle properties are plotted.

Figure 11 (left panel) shows the behaviour of the primary polydispersity, given by the average of the geometric standard deviation of primary diameters in a particle. The 'time through reactor' coordinate refers to the axial position in the reactor, whereas the 'time' axis is the transient response. There is good agreement between the network and PFR solutions in early reactor times (i.e. initial section of PFR length). This agreement appears to decay as coagulation accelerates, similar to Figures 9 and 10.

The degree of sintering (Figure 11, right panel) lies on $[0, 1.0]$ where 0 is equivalent to two primaries in point contact (i.e. no sintering) and 1.0 is full-coalescence [43]. In this particular example, the growth by coagulation and sintering under similar timescales [29] causes aggregates of partially-sintered primaries to form, thus depression in the sintering level in both time trajectories is observed.

The primary polydispersity and sintering level are parameters which cannot be obtained

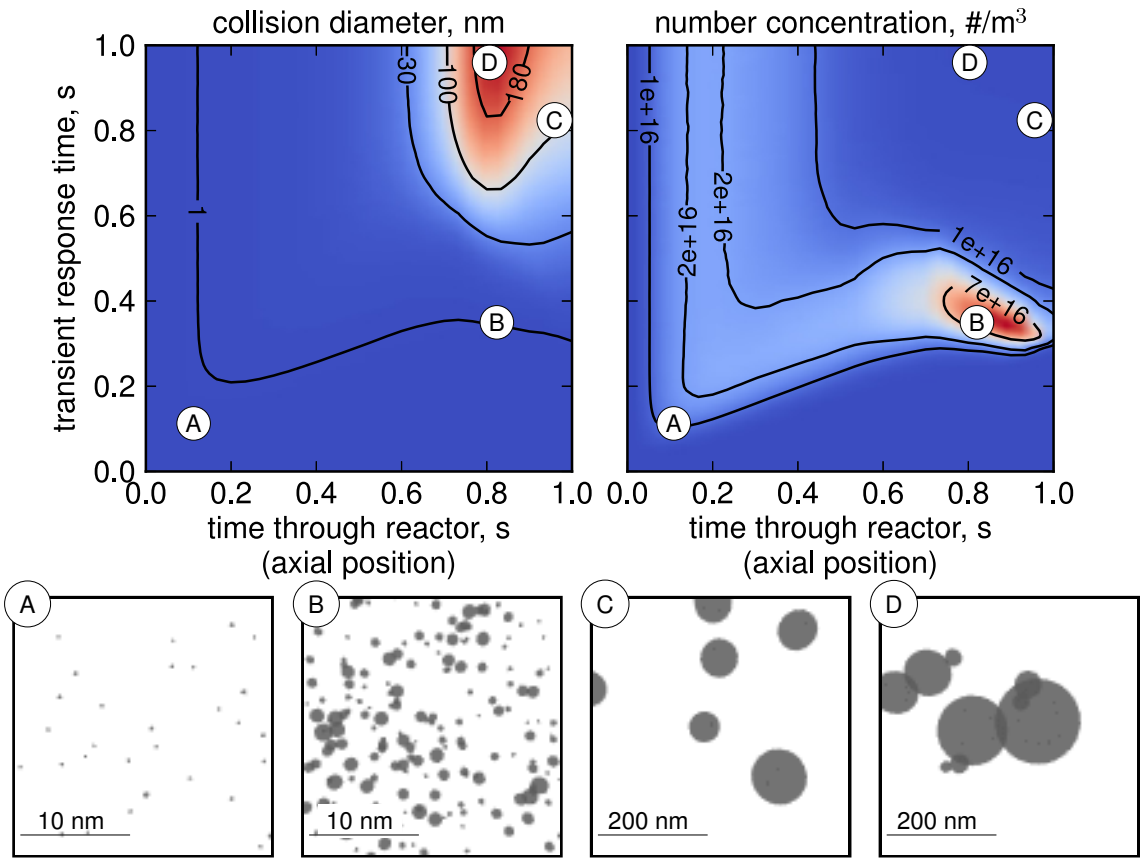

Figure 12: *Contour plots of transient evolution of average collision diameter and particle number concentration. Insets illustrate the particle ensemble state with TEM-style images at the given reactor time (i.e. axial position) and transient response time coordinates, generated using POV-Ray [39].*

by using deterministic population balance modelling techniques. Stochastic methods using the binary-tree particle model additionally can interrogate the particle ensemble to generate images of sample particle structures. This is illustrated in Figure 12, where sample TEM-style images are generated for specific PFR axial position times and transient response times.

The collision diameter (Figure 12 left panel) and number concentration (Figure 12 right panel) are presented to give representative values of particle size and quantity as a function of reactor position and transient response time. Panel A represents the initial generation of 'seed' particles, which are transported through the network until point B, where the temperature profile causes further rapid nucleation and surface growth. The spike in number concentration at B increases the coagulation rate, causing aggregates to form (Panel D). If particles are transported to the outlet of the reactor, the final temperature increase sinters the particles back to spheres (Panel C).

The temporal evolution of these quantities illustrates the power of the methodology developed in the present work: using a fully-coupled model incorporating gas-phase kinetics and a multidimensional particle model enables an unprecedented amount of detail of par-

ticle composition, size and structure to be captured in a transient flow reactor.

5 Conclusions

This work has presented an algorithm to solve a reactor network with a fully-coupled gas-phase and stochastic population balance solver. The algorithm uses sequential modular simulation to solve the network in a stepwise fashion. Novel processes for accounting for particle in- and outflow were proposed.

The convergence properties of the network solution algorithm were assessed in order to identify suitable choices for numerical parameters. A choice of 4096 computational particles was recommended to minimise systematic error. A new algorithm for simulating particle outflow (termed volume 'rescaling') was also shown to be advantageous in reducing statistical error. Two algorithms for coagulation were considered: the direct simulation algorithm (DSA) and a stochastic weighted algorithm (SWA). It was found that the SWA algorithm showed superior reduction of systematic and statistical error for almost all properties of the particle ensemble. The direct simulation algorithm was found to be unsuitable for networks with strong feedback.

To illustrate potential applications of this methodology, a plug flow reactor was approximated as a linear series of perfectly-stirred reactors. The number of PSRs required to approximate such a system as a function of coagulation rate was first evaluated. The system was then solved using a multivariate silicon particle model to simulate the start-up of a flow reactor system.

The coupling of a stochastic methods to computational fluid dynamics codes is still very-much in its infancy. As no other method of solving the population balance equation is currently able to use detailed multivariate particle models such as the binary-tree model used in the present work; it is anticipated that stochastic methods will play a stronger role in process modelling. This work has contributed to the understanding of numerical aspects of such approaches.

6 Acknowledgements

W.J.M. acknowledges financial support provided by the Cambridge Australia Trust. W.J.M. and M.K. are grateful for the support of the Weierstrass Institute for Applied Analysis and Stochastics (WIAS) in Berlin and thank R.I.A. Patterson and W. Wagner for useful discussions on the topic. M.K. gratefully acknowledges the DFG Mercator programme and the support of CENIDE at the University of Duisburg Essen.

References

[1] J. Akroyd, A. J. Smith, L. R. McGlashan, and M. Kraft. Numerical investigation of DQMoM-IEM as a turbulent reaction closure. *Chemical Engineering Science*, 65 (6):1915–1924, 2010.

[2] J. Akroyd, A. Smith, R. Shirley, L. McGlashan, and M. Kraft. A coupled CFD-population balance approach for nanoparticle synthesis in turbulent reacting flows. *Chemical Engineering Science*, 66(17):3792–3805, 2011.

[3] A. H. Alexopoulos, P. Pladis, and C. Kiparissides. Nonhomogeneous mixing population balance model for the prediction of particle size distribution in large scale emulsion polymerization reactors. *Industrial & Engineering Chemistry Research*, (In press), 2013.

[4] M. Balthasar and M. Kraft. A stochastic approach to calculate the particle size distribution function of soot particles in laminar premixed flames. *Combustion and Flame*, 133(3):289–298, 2003.

[5] S. Bermingham, P. Verheijen, and H. Kramer. Optimal design of solution crystallization processes with rigorous models. *Chemical Engineering Research and Design*, 81(8):893–903, 2003.

[6] F. Bezzo and S. Macchietto. A general methodology for hybrid multizonal/CFD models: Part II. Automatic zoning. *Computers & Chemical Engineering*, 28(4): 513–525, 2004.

[7] F. Bezzo, S. Macchietto, and C. Pantelides. A general methodology for hybrid multizonal/CFD models: Part I. Theoretical framework. *Computers & Chemical Engineering*, 28(4):501–511, 2004.

[8] A. Bhave and M. Kraft. Partially stirred reactor model: Analytical solutions and numerical convergence study of a PDF/Monte Carlo method. *SIAM Journal on Scientific Computing*, 25(5):1798–1823, 2004.

[9] G. Bird, M. Gallis, J. Torczynski, and D. Rader. Accuracy and efficiency of the sophisticated direct simulation Monte Carlo algorithm for simulating noncontinuum gas flows. *Physics of Fluids*, 21:017103, 2009.

[10] A. Braumann, M. Goodson, M. Kraft, and P. Mort. Modelling and validation of granulation with heterogeneous binder dispersion and chemical reaction. *Chemical Engineering Science*, 62(17):4717–4728, 2007.

[11] V. S. Buddhiraju and V. Runkana. Simulation of nanoparticle synthesis in an aerosol flame reactor using a coupled flame dynamics–monodisperse population balance model. *Journal of Aerosol Science*, 43(1):1–13, 2012.

[12] CD-adapco. STAR-CCM+ v7.02 Help, 2012.

[13] M. Celnik, R. Patterson, M. Kraft, and W. Wagner. Coupling a stochastic soot population balance to gas-phase chemistry using operator splitting. *Combustion and Flame*, 148(3):158–176, 2007.

[14] M. Celnik, R. Patterson, M. Kraft, and W. Wagner. A predictor-corrector algorithm for the coupling of stiff ODEs to a particle population balance. *Journal of Computational Physics*, 228(8):2758–2769, 2009.

[15] D. Chen, Z. Zainuddin, E. Yapp, J. Akroyd, S. Mosbach, and M. Kraft. A fully coupled simulation of PAH and soot growth with a population balance model. *Proceedings of the Combustion Institute*, 34:1827–1835, 2013. URL http://dx.doi.org/10.1016/j.proci.2012.06.089.

[16] A. Eibeck and W. Wagner. An efficient stochastic algorithm for studying coagulation dynamics and gelation phenomena. *SIAM Journal on Scientific Computing*, 22(3): 802–821, 2001.

[17] H. Fogler. *Elements of Chemical Reaction Engineering*. Pearson, New Jersey, 2006.

[18] M. Frenklach and S. Harris. Aerosol dynamics modeling using the method of moments. *Journal of Colloid and Interface Science*, 118(1):252–261, 1987.

[19] A. Garcia, C. van den Broeck, M. Aertsens, and R. Serneels. A Monte Carlo simulation of coagulation. *Physica A*, 143(3):535–546, 1987.

[20] M. Goodson and M. Kraft. An efficient stochastic algorithm for simulating nanoparticle dynamics. *Journal of Computational Physics*, 183(1):210–232, 2002.

[21] R. Irizarry. Fast compartmental Monte Carlo simulation of population balance models: Application to nanoparticle formation in nonhomogeneous conditions. *Industrial & Engineering Chemistry Research*, 51(47):15484–15496, 2012.

[22] T. Johannessen, S. E. Pratsinis, and H. Livbjerg. Computational fluid-particle dynamics for the flame synthesis of alumina particles. *Chemical Engineering Science*, 55(1):177–191, 2000.

[23] A. Kazakov and M. Frenklach. Dynamic modeling of soot particle coagulation and aggregation: Implementation with the method of moments and application to high-pressure laminar premixed flames. *Combustion and Flame*, 114(3):484–501, 1998.

[24] R. Körmer, M. Jank, H. Ryssel, H. Schmid, and W. Peukert. Aerosol synthesis of silicon nanoparticles with narrow size distribution–Part 1: Experimental investigations. *Journal of Aerosol Science*, 41(11):998–1007, 2010.

[25] F. E. Kruis, J. Wei, T. van der Zwaag, and S. Haep. Computational fluid dynamics based stochastic aerosol modeling: Combination of a cell-based weighted random walk method and a constant-number Monte-Carlo method for aerosol dynamics. *Chemical Engineering Science*, 70:109–120, 2012.

[26] J. Li, B. Freireich, C. Wassgren, and J. D. Litster. A general compartment-based population balance model for particle coating and layered granulation. *AIChE Journal*, 58(5):1397–1408, 2012.

[27] D. L. Marchisio and R. O. Fox. Solution of population balance equations using the direct quadrature method of moments. *Journal of Aerosol Science*, 36(1):43–73, 2005.

[28] W. Menz and M. Kraft. A new model for silicon nanoparticle synthesis. *Combustion & Flame*, 160:947–958, 2013.

[29] W. Menz and M. Kraft. The suitability of particle models in capturing aggregate structure and polydispersity. *Aerosol Science and Technology*, 47:734–745, 2013.

[30] W. Menz, S. Shekar, G. Brownbridge, S. Mosbach, R. Körmer, W. Peukert, and M. Kraft. Synthesis of silicon nanoparticles with a narrow size distribution: a theoretical study. *Journal of Aerosol Science*, 44:46–61, 2012.

[31] W. Menz, R. Patterson, W. Wagner, and M. Kraft. Application of stochastic weighted algorithms to a multidimensional silica particle model. *Journal of Computational Physics*, 248:221–234, 2013.

[32] N. Morgan, C. Wells, M. Goodson, M. Kraft, and W. Wagner. A new numerical approach for the simulation of the growth of inorganic nanoparticles. *Journal of Computational Physics*, 211(2):638–658, 2006.

[33] S. Mosbach, M. S. Celnik, A. Raj, M. Kraft, H. R. Zhang, S. Kubo, and K.-O. Kim. Towards a detailed soot model for internal combustion engines. *Combustion and Flame*, 156(6):1156–1165, 2009.

[34] O. Muscato, V. Di Stefano, and W. Wagner. A variance-reduced electrothermal Monte Carlo method for semiconductor device simulation. *Computers & Mathematics with Applications*, 65:520–527, 2013.

[35] R. Patterson and W. Wagner. A stochastic weighted particle method for coagulation–advection problems. *SIAM Journal on Scientific Computing*, 34(3):290–311, 2012.

[36] R. Patterson, J. Singh, M. Balthasar, M. Kraft, and J. Norris. The linear process deferment algorithm: A new technique for solving population balance equations. *SIAM Journal on Scientific Computing*, 28(1):303, 2006.

[37] R. Patterson, J. Singh, M. Balthasar, M. Kraft, and W. Wagner. Extending stochastic soot simulation to higher pressures. *Combustion and Flame*, 145(3):638–642, 2006.

[38] R. Patterson, W. Wagner, and M. Kraft. Stochastic weighted particle methods for population balance equations. *Journal of Computational Physics*, 230:7456–7472, 2011.

[39] Persistence of Vision Pty. Ltd. Persistence of Vision Raytracer (Version 3.6), 2004. URL http://www.povray.org/.

[40] J. Pyykönen and J. Jokiniemi. Computational fluid dynamics based sectional aerosol modelling schemes. *Journal of Aerosol Science*, 31(5):531–550, 2000.

[41] Reaction Design. CHEMKIN Software Theory Manual, 2011.

[42] K. Sabelfeld, S. Rogasinsky, A. Kolodko, and A. Levykin. Stochastic algorithms for solving Smolouchovsky coagulation equation and applications to aerosol growth simulation. *Monte Carlo Methods Applied*, 2(1):41–87, 1996.

[43] M. Sander, R. West, M. Celnik, and M. Kraft. A detailed model for the sintering of polydispersed nanoparticle agglomerates. *Aerosol Science and Technology*, 43(10): 978–989, 2009.

[44] M. Sander, R. Patterson, A. Braumann, A. Raj, and M. Kraft. Developing the PAH-PP soot particle model using process informatics and uncertainty propagation. *Proceedings of the Combustion Institute*, 33(1):675–683, 2011.

[45] T. Seto, M. Shimada, and K. Okuyama. Evaluation of sintering of nanometer-sized titania using aerosol method. *Aerosol Science and Technology*, 23(2):183–200, 1995.

[46] S. Shekar, W. Menz, A. Smith, M. Kraft, and W. Wagner. On a multivariate population balance model to describe the structure and composition of silica nanoparticles. *Computers & Chemical Engineering*, 43:130–147, 2012.

[47] S. Shekar, A. Smith, W. Menz, M. Sander, and M. Kraft. A multidimensional population balance model to describe the aerosol synthesis of silica nanoparticles. *Journal of Aerosol Science*, 44:83–98, 2012.

[48] J. Singh, M. Balthasar, M. Kraft, and W. Wagner. Stochastic modeling of soot particle size and age distributions in laminar premixed flames. *Proceedings of the Combustion Institute*, 30(1):1457–1465, 2005.

[49] J. Wen, M. Thomson, S. Park, S. Rogak, and M. Lightstone. Study of soot growth in a plug flow reactor using a moving sectional model. *Proceedings of the Combustion Institute*, 30(1):1477–1484, 2005.

[50] J. Wu, H. Nguyen, and R. Flagan. A method for the synthesis of submicron particles. *Langmuir*, 3(2):266–271, 1987.

[51] R. Zauner and A. G. Jones. On the influence of mixing on crystal precipitation processes–application of the segregated feed model. *Chemical Engineering Science*, 57(5):821–831, 2002.

[52] H. Zhao and C. Zheng. A population balance-Monte Carlo method for particle coagulation in spatially inhomogeneous systems. *Computers & Fluids*, 71:196–207, 2013.

[53] H. Zhao, F. E. Kruis, and C. Zheng. A differentially weighted monte carlo method for two-component coagulation. *Journal of Computational Physics*, 229(19):6931–6945, 2010.